First-principles cluster expansion study of missing-row reconstructions of fcc (110) surfaces

Wei Chen, David Schmidt, William F. Schneider, and C. Wolverton

Phys. Rev. B **83**, 075415 — Published 14 February 2011

DOI: 10.1103/PhysRevB.83.075415

First-principles Cluster Expansion Study of Missing-row Reconstructions of fcc (110) Surfaces

Wei Chen, C. Wolverton[1], David Schmidt[2], William Schneider[2,3]

[1] Department of Materials Science and Engineering, Northwestern University, Evanston, IL 60208, USA

[2] Department of Chemical and Biomolecular Engineering, University of Notre Dame, Notre Dame, IN, 46556, USA

[3] Department of Chemistry and Biochemistry, University of Notre Dame, Notre Dame, IN, 46556, USA

Theoretical prediction of surface reconstructions is difficult and rare due to the extremely large phase space of possible 2D atomic surface configurations. Here, we demonstrate how a first-principles cluster expansion (CE) method can be used to identify a particular class of stable surface reconstructions involving the surface ordering of atoms and vacancies without any empirical input. We apply the method to late transition metal (110) surfaces and correctly demonstrate the reconstruction tendency for 5d metals to reconstruct in the "missing row" (1×2) structure, but not 3d or 4d metals. In addition to providing physical insight into the origin of the reconstruction tendency, the CE also allows us to predict the finite temperature stability of the reconstruction, the order-disorder (1×2)→(1×1) transition temperature, and the equilibrium shape of the surface islands.

Surface science studies have provided many interesting examples of surface reconstructions.[1-4] One prominent instance is the (1×2) missing-row (MR) reconstruction of late 5d transition metal (110) surfaces (Fig. 1). Properties related to the MR reconstruction, such as the critical phenomena at transition temperatures, can be well described by theories based on symmetry principles.[5, 6] Despite their successes, these theories are limited in the sense that they are unable to answer the following question: Which metals reconstruct and which do not? In other words, these approaches still require experimental input to differentiate the unreconstructed Cu(110) surface from the reconstructed Au(110) surface. On the other hand, first-principles methods, based on density functional theory (DFT), are effective in identifying the relative energetic stability of reconstructed or unreconstructed surfaces.[7] DFT methods have also contributed to a better understanding of MR atomic-scale structure and even the physical origin of MR reconstruction.[8] However, DFT studies share a common drawback. That is, the atomic-scale structure of the stable surface reconstruction cannot be predicted *a priori*, but rather must be experimentally measured. A truly predictive method to determine surface reconstructions would require an efficient method to search through the vast configurational space of possible surface reconstruction for the lowest-energy reconstruction. This type of search strategy is made difficult by the astronomical number of configurations possible in the phase space, which cannot be sampled exhaustively. Adding to the difficulty is that DFT calculations of large supercells needed to simulate complex surface reconstructions may be computationally prohibitive. Here, we illustrate how a combination of first-principles DFT calculations, a cluster expansion (CE), and Monte Carlo (MC) simulations may be used to overcome these difficulties for a specific

class of surface reconstructions involving surface ordering of atoms and vacancies. The CE based method has been successfully applied to a wide range of surface problems including adsorbates ordering, surface segregation and surface phase diagram.[9-14] We focus on the MR reconstruction of fcc (110) surfaces to illustrate the effectiveness of this method to predict the existence/absence of reconstruction tendencies for 3d/5d metals. Using the first-principles cluster expansion, we are able to search through a very large number of possible reconstructions, and correctly predict the experimentally-observed surface reconstruction as the low-energy ground state. In addition to providing physical insight into the origin of the reconstruction tendency, the combination of DFT+CE+MC also allows us to predict quantities that would be impossible to obtain from DFT alone, namely the finite temperature stability of the reconstruction, the order-disorder $(1\times2)\rightarrow(1\times1)$ transition temperature, and the equilibrium shape of the surface islands.

We use the cluster expansion formalism[15] to treat the surface reconstruction as a two-dimensional pseudo-binary ordering problem of atoms and vacancies on a single surface layer. In this generalized Ising-like model, a surface site occupied by an atom is assigned a spin occupation variable S_i=+1and a vacant site is assigned S_i=−1. The total energy of any configuration σ for the surface can be written as

$$E(\sigma) = J_0 + \sum_i J_i S_i(\sigma) + \sum_{j<i} J_{ij} S_i(\sigma) S_j(\sigma) + \sum_{k<j<i} J_{ijk} S_i(\sigma) S_j(\sigma) S_k(\sigma) + \cdots \qquad (1)$$

where the coefficients J_f are effective cluster interactions (ECI) associated with clusters of lattice sites (pairs, triplets, quadruplets, etc). The spin products of clusters form an orthonormal and complete basis set in the space of all 2^N configurations, making the expansion mathematically rigorous, but not necessarily convergent. In practice, the

expansion is often truncated with only a relatively small number of clusters, typically resulting in a converged CE. An optimal set of ECIs is obtained by minimizing the cross-validation score[16] of the CE fitting across DFT energies for a set of surface atom/vacancy configurations.

For our DFT calculations, we use a slab model for the surface structures. The number of atomic layers (11~14 layers for different elements) and the thickness of the vacuum region (10Å) were carefully optimized to make the (110) surface energy converged to at least 1 meV/surface site. DFT calculations were carried out by Vienna *ab initio* Simulation Package (VASP) using the projector augmented wave (PAW) method. The generalized gradient approximation of Perdew and Wang[17] was used to approximate the electronic exchange and correlation. The plane wave basis set for the electronic wave functions was defined by a cutoff energy of 400 eV and the Brillouin-zone integrations were sampled using roughly constant Monkhorst-Pack k-point meshes corresponding to a 21×21×1 grid for a 1×1 unit cell. The formation energies of various structures consisting of ordered arrangements of atoms/vacancies on a (110) surface are cluster expanded with 2D clusters. The formation energies are referenced to "pure" surfaces with full "coverages" of atoms or vacancies. These are identically terminated surfaces differing by one layer of atoms in the supercells. The formation energy of a surface structure with an atom coverage θ is defined as follows:

$$E_F(\theta) = [E(\theta) - (1-\theta)E_{n-1}^{1\times1} - \theta E_n^{1\times1}] / N \qquad (2)$$

where E(θ) is the total energy for the surface structure, and $E_{n-1}^{1\times1}$ and $E_{n}^{1\times1}$ are the energies for the unreconstructed surfaces with n-1 and n layers of atoms, respectively. The formation energies are normalized to energy per surface site.

We have studied the (110) surfaces of four metals using our first-principles cluster expansion method: Ag, Au, Cu and Pt. We note that two of these metals have been observed to exhibit the MR reconstruction (Au and Pt) while two do not show the MR reconstruction (Cu and Ag).[18, 19] In our CE, we include the "empty" and point clusters, as well as pairs, triplets, and quadruplets. About 50 DFT energies are needed to obtain a converged cluster expansion with a typical cross-validation score of 2~7 meV/surface site for each metal surface. In the DFT calculations, the bottom three layers of atoms are fixed, while the remaining layers are relaxed. The effect of surface multilayer relaxation is thereby included in the surface cluster expansion. To find the T=0 K stable reconstruction structure, the formation energies of supercells up to 16 surface sites (about 2^{16} surface structures) were explicitly evaluated by surface CE.

We first illustrate our method for the Ag(110) and Cu(110) surfaces in Fig. 2(a) and 2(b). The blue dots are formation energies of different atom/vacancy surface configurations predicted from the CE Hamiltonian. The green line shows the lowest energy reconstruction configurations as a function of coverage, which forms a "convex hull" of ground state structure for the surface. In these systems, all values of the formation energy in Eq. (2) are positive, indicating that the creation of any arrangement of vacancies on the surface of the unreconstructed surface tends to *increase* the energy of the surface. The ground state convex hull is a straight line connecting structures at θ=0 and θ=1, which both correspond to the unreconstructed surface. Thus, in these cases, our DFT+CE

method clearly predicts the absence of reconstruction for Ag(110) and Cu(110), in agreement with observations.[20, 21]

Next, we illustrate our method for Au(110) and Pt(110). In the case of Cu and Ag, the interactions between surface atoms are uniformly attractive, and introduction of a vacancy or vacancy array is always energetically costly. However, for Au and Pt(110) surface, this simple picture is not correct. For these metals, the convex hull is no longer a simple line connecting the θ=0 and θ=1 unreconstructed states. Instead, there is a phase at θ=1/2 which appears on the ground state convex hull for both Pt(110) and Au(110) (Figs. 2(c) and 2(d)). This existence of this θ=1/2 structure on the convex hull indicates that there is an ordered arrangement of vacancies and metal atoms at the surface that is thermodynamically stable at T=0 K, and serves to lower the energy of the unreconstructed state. In other words, Figs. 2(c) and 2(d) indicates a stable reconstruction exists for these surfaces. The stable θ=1/2 structure predicted by the CE is the (1×2) MR structure, where every other row of atoms along $[1\bar{1}0]$ is missing for the Au(110) and Pt(110) surface. We emphasize here that these structures were obtained directly from the CE, without the need for guessing any particular surface structures in advance. We also note from Fig. 2(c) and 2(d) that there are a number of surface structures whose formation energies seem to be almost linearly along the tie line connecting the MR(1×2) structure with the unreconstructed (1×1) structure at θ=0 or θ=1. These are missing-row-like structures, involving a periodic arrangement of metal rows and empty rows. They all have a nearest-neighbor pair correlation of 1, corresponding to completely filled or completely empty rows along the nearest neighbor directions. However, these low-energy structures have unit cells of (1×n) types with longer periods

(n>2) than the (1×2) structure and the (1×2) MR structure is the global energy minimum for these (110) surfaces. The prediction of the stability of the (1×2) MR structure for Pt(110) and Au(110) but not Ag(110) or Cu(110) from our first-principles cluster expansion search is in agreement with existing experimental results.[18, 22, 23]

We can understand the reconstruction tendencies of the various transition metals in terms of the values of the cluster expansion interactions. In particular, the formation of the MR structure for 5d transition metals but not for 3d and 4d transition metals is a result of a large difference in the inter-row (along$[1\bar{1}0]$) interactions. Fig. 3 shows the clusters used for Au(110), which include pair, triplet and quadruplet. Cluster selections for other surfaces are similar to those for Au(110). The ECIs of the major pair interactions are listed in Table I. For the pair interactions, a positive ECI means an ordering tendency (a preference for metal-vacancy pairs) whereas a negative value means a clustering tendency (a preference for metal-metal or vacancy-vacancy pairs). The four studied metals all have a large negative ECI for the nearest neighbor pair, showing a strong clustering tendency along the row ([001]). The interesting distinction between 5d and non-5d metals is in the *inter-row* pair interactions. The 5d metals have a strong, positive ordering-type interaction between rows, indicative of a preference for alternating metal/vacancy rows. The 3d and 4d metals have very weak inter-row pair interactions near zero, implying essentially no energetic preference for metal-metal or metal-vacancy pairs between rows, and hence results in no strong preference for a (1×2) MR reconstruction. For all four metals, we also calculated the formation energy of random atom/vacancy configurations on the (110) surfaces using CE Hamiltonians (Fig. 2). Despite the fact that MR structure has a negative formation energy for 5d metal (110)

surfaces (indicating this *ordered* arrangement of vacancies on the surface is lower in energy than the unreconstructed surface), the formation energy of random (110) surfaces is positive (indicating that a *disordered* arrangement of vacancies is higher in energy than the unreconstructed surface). The interesting difference in formation energy is also due to the strong anisotropy of ordering interactions: a clustering tendency along the rows, but an ordering tendency between rows.

To this point, we have used the first-principles CE to assess the T=0 K stability of the MR reconstruction. Combining the CE energies with grand canonical Monte Carlo simulations, we can assess the finite-temperature stability of the surface reconstruction. We have performed Monte Carlo simulations of Au(110) using a simulation cell size of 68×50 surface sites. For Pt(110), a coupled deconstruction and 3D roughing transition proceed at the same temperature[24]. Our CE approach is capable of describing order/disorder transition on the surface layer; however, the 3D roughening transition is outside the scope of the current manuscript, as this transition would require an energy model with interactions among several top layers of atoms. The simulation of Au (110) was carried out by fixing the chemical potential difference between atom and vacancy at zero, which allows the surface to adopt its equilibrium configuration on an unlimited bulk reservoir with equal energy penalty of atom and vacancy. We have run simulations both by raising the temperature from 0 K and also by cooling down from 2000 K, with an initial configuration of (1×2) MR structure for the heating runs and random surface at ½ coverage for both types of runs. All simulations give similar results and stabilize the (1×2) MR structure at 0 K. We define a long-range order (LRO) parameter, η, as the mean occupancy difference between odd and even numbered rows, and monitor this LRO

parameter as a function of temperature. The (1×2) MR structure (|η|=1) is very stable at lower temperatures and the LRO parameter decreases only slowly at low temperature. At higher temperatures, the ordered structure gives way to a disordered (1×1) phase and LRO parameter drops to 0 (Fig. 4). The Monte Carlo simulation based on first-principles energetics successfully reproduces an order-disorder transition of the (1×2) MR reconstruction and is in agreement with experimental observations, in which the ½-order spots disappear in LEED pattern and primitive (1×1) structures are observed[6]. The transition temperature from our simulation is about 1150 K, which is higher than the experimental value of 735 K[22]. This type of overestimation of order-disorder transition temperatures from first-principles is common in calculations of bulk alloy phase diagrams, particularly in cases where vibrational entropy ignored [25, 26]. A previous study of the MR reconstruction using embedded atom potentials has pointed to the importance of both atomic relaxation as well as vibrational entropy in describing these transitions[27]. Because we have included atomic relaxation in our calculations, we hypothesize that the vibrational thermodynamics of this system might serve to lower the calculated transition temperature. This effect of vibrational entropy on phase stability has been seen previously in bulk systems as well[28-30]. Using the first-principles direct force-constant method[31, 32], we have calculated the vibrational entropy for the nonreconstructed (1×1) and (1×2) MR structure of Au(110). A 3×3×1 supercell of (1×1) slab and a 3×2×1 supercell of (1×2) slab were used in the phonon calculations. Five evenly distributed perturbations around the equilibrium positions with a step size of 0.03Å were applied to obtain the forces using harmonic model. The results show that the vibrational entropy difference between the two structures is about 0.24 k_B/surface site and is nearly constant

above T~300K, with a higher entropy for the (1×1) structure than for the (1×2) MR structure. We note two geometrical factors which could contribute to the vibrational entropy difference between the (1x1) and the (1x2) MR structures. First, the inward relaxation of a top layer atom is much larger in the (1x2) MR structure (~20%) than that it is in the (1x1) structure (~14%). A stronger bond between the surface layer atom and its nearest neighbor atoms in the second layer is thus expected for the (1x2) MR structure, which results in higher frequency vibrations and a lower entropy. Second, disordering the MR structure requires the formation of metal-metal bonds between rows, at the expense of bonds within a row. The length of the former bonds are larger (by a factor of $\sqrt{2}$) than the latter, which induces softer bonds and a higher vibrational entropy. Thus, our DFT calculations show that the inclusion of vibrational entropy will serve to lower the calculated transition temperature, bring it in closer agreement to experiment.

Short-range order is significant for the MR reconstructed surfaces above the transition temperature. There are still short segments of "rows" and small remnants of the (1×2) MR structure from our MC simulations (Fig. 4). We define the correlation of a cluster of surface sites as the average of spin product for that cluster over the whole surface. The correlations of most clusters in the surface CE decrease with the increase of temperature, which shows a tendency towards disorder on the surface (Fig. 5). However, a non-zero value of the correlation above transition temperature indicates the existence of short-range order for the surface. We found pair correlations, especially the nearest neighbor pair along the row, are strong even above the transition temperature.

We have also used our first-principles CE to describe equilibrium island shapes on the surface. Because an equilibrium island should adopt a shape to minimize its total step

energy, the shape can be estimated from the ratio of the step energies for different sides of the island. To calculate step energy from DFT, the supercell should be large enough in two dimensions to avoid the interactions between neighboring steps. It is very expensive to do such calculations as the supercell can easily contain hundreds of atoms. A surface step can be thought of as the boundary between occupied and vacant regions on a surface, which can be treated a configuration of atom and vacancies. The step energy along any directions on the surface can therefore be efficiently obtained from the CE Hamiltonian. We have calculated the step energies along the [001] and $[1\bar{1}0]$ directions for Ag(110) and Au(110) surfaces using our CE. To validate the accuracy of these CE step energies, we also compute the step energies directly from DFT supercell calculations where possible. Since the Ag(110) surface does not reconstruct, a simple step between two flat, unreconstruct planes was considered. The shape of the equilibrium island shape on the (110) surface is estimated from the anisotropic ratio of these step energies (Table II). We find that CE step energy is able to reproduce the DFT energy very well and gives an accurate ratio of step energies. However, the supercell (1×8) used here in the DFT calculations is too small to consider the relaxation along the step or avoid the interactions between steps in the direct DFT calculations, resulting in a higher step energy. The CE energies can be easily extended to much larger 100×50 supercells (Table II), which is large enough to include these effects. We got lower step energies from CE using these huge supercells as a result. The calculation of such supercell is beyond the ability of DFT. The value of 5.5 for Ag(110) island is in reasonable agreement with experimental results, which is about 3 at 200K.[33]

We also demonstrate the utility of the first-principles CE to study the properties of surface defects. We have calculated surface vacancy formation energy on unreconstructed Au(110) from both CE Hamiltonian and DFT. Both calculations are from a 4×4 supercell (176 atoms and 1 surface vacancy) and are able to get well converged results with respect to the cell size. The CE energy is 0.854eV/vacancy, while the DFT energy is 0.849eV/vacancy. First-principles CE is able to obtain results with DFT accuracy, but without lengthy calculations. Similarly, we can also obtain the Au adatom binding energy on unreconstructed Au(110). The CE binding energy is -0.715eV/atom, which is comparable to DFT energy -0.760eV/atom. The formation energy of surface defects is important in understanding the diffusion mechanism on those surfaces.[34]

In conclusion, we have illustrated a method for determining the stable surface reconstruction orderings and studying the finite temperature stability of reconstructions by a first-principles cluster expansion approach. We studied the (110) surfaces of four late transition metals, and correctly predict the presence (absence) of the MR reconstruction for Au and Pt (Cu and Ag), without any empirical input. We have also shown that the first-principles CE method facilitates the study of finite-temperature surface phase transformations and surface morphology. The general method we have described here is applicable to a class of surface reconstruction problems that can be modeled as the ordering of atoms and vacancies.

This work is supported by National Science Foundation under contract No. CBET-0730841 and No. CBET-0731020.

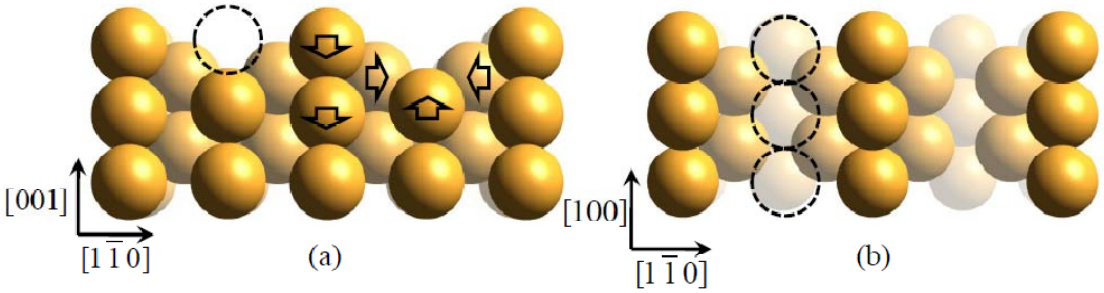

Fig. 1 Side view (a) and top view (b) of the (1×2) missing-row reconstruction on Au and Pt (110) surfaces. The arrows illustrate the relaxation of surface atoms. The dashed circles are the positions where the "missing" atoms from an unreconstructed (1×1) surface.

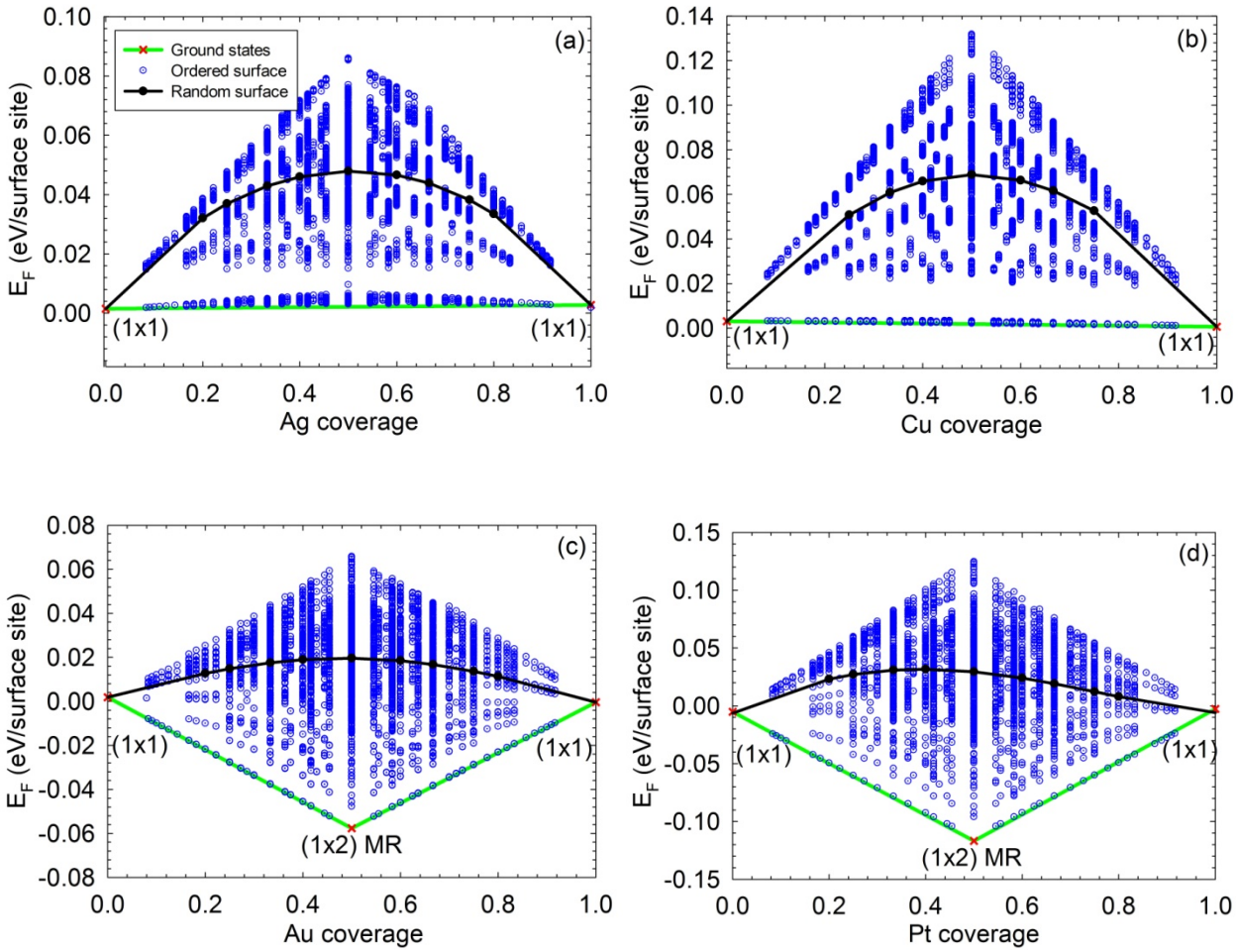

Fig. 2 Ground state diagrams for (a) Ag, (b) Cu, (c) Au and (d) Pt(110) surface with predicted formation energies for ordered (blue dots) and random (black line) surface from first-principles cluster expansion. The green lines show the lowest energy reconstruction configurations as a function of coverage. Au and Pt(110) surfaces show (1×2) MR reconstruction, but Ag and Cu(110) surfaces do not.

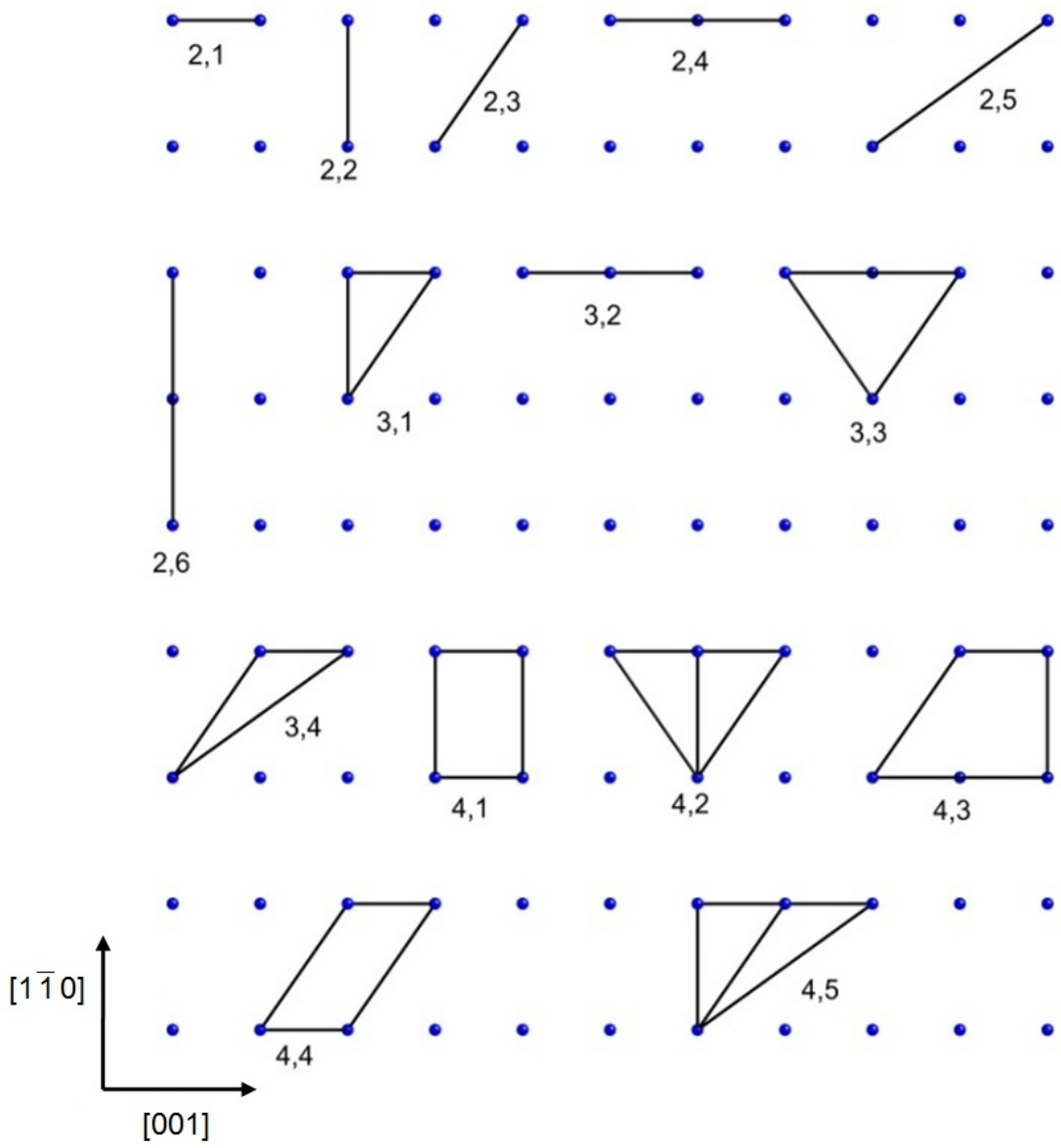

Fig. 3 Clusters used in CE for Au(110) surface. For each cluster, the first number is the number of sites within the cluster and the second number differentiates clusters of the same class

Table I. Trend in pair ECIs for the (110) surfaces.

	Missing Row Observed?	$J_{2,1}$	$J_{2,2}$	$J_{2,3}$	$\lvert J_{2,1}/J_{2,2}\rvert$	$\lvert J_{2,1}/J_{2,3}\rvert$
		meV/pair surface site				
Au	Y	-50.40	7.71	8.93	6.54	5.64
Pt	Y	-106.95	14.73	9.99	7.26	10.71
Ag	N	-40.90	1.24	-0.56	33.12	73.17
Cu	N	-62.30	-1.73	1.50	36.01	41.53

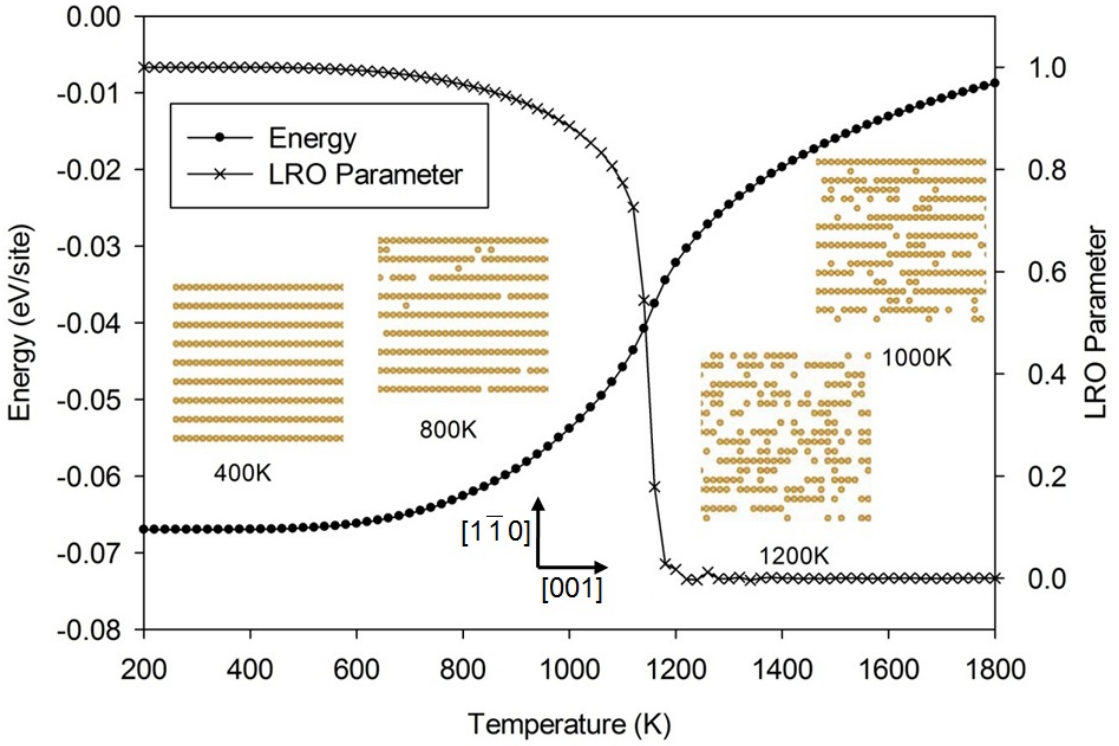

Fig.4 Change of energy and long-range order parameters with temperature for Au(110) MR structure from Monte Carlo simulation. Together with the snapshots of surface configuration at different temperatures, the results show an order-disorder transition of the MR structure.

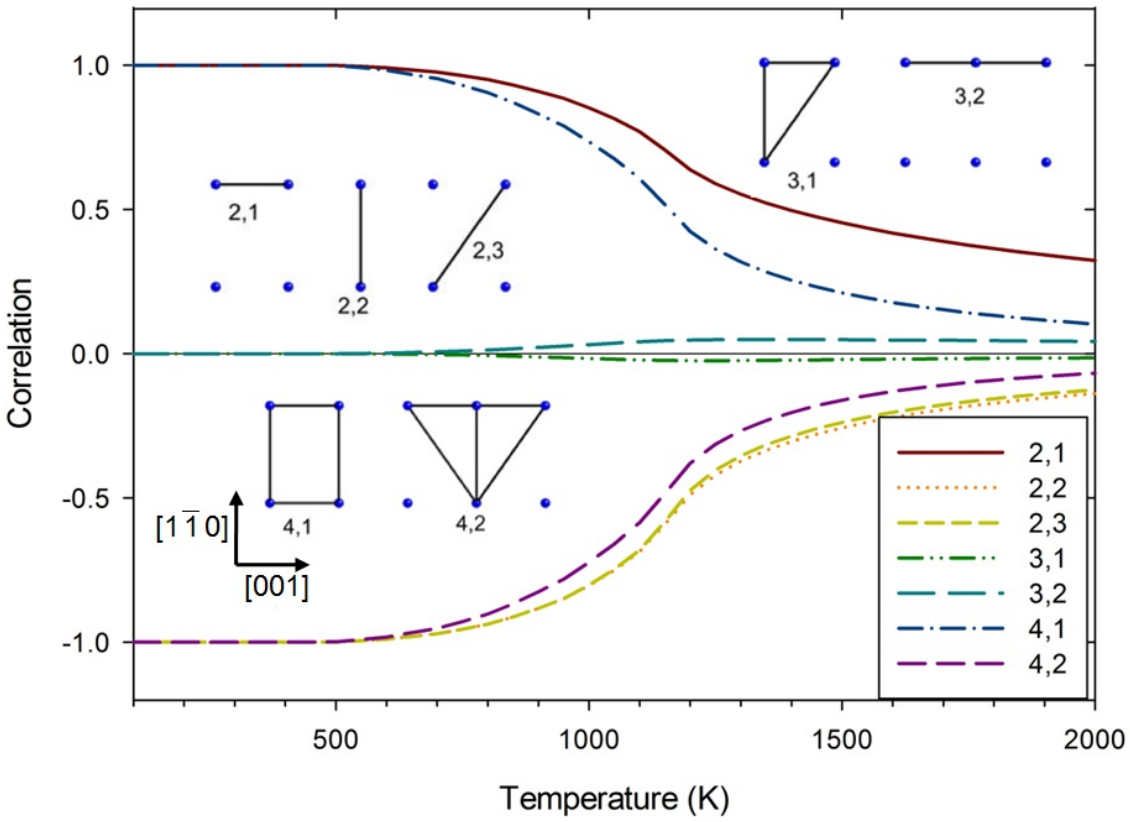

Fig. 5 Change of cluster correlations with temperature for Au(110) surface. The strong pair correlations are related to the short range order of the surface above transition temperature.

Table II. Step energy of (110) surfaces

	Surface structure	*Number of Surface sites*	$\gamma_{[001]}$ (eV/Å)	$\gamma_{[1\text{-}10]}$ (eV/Å)	$\gamma_{[001]}/\gamma_{[1\text{-}10]}$
Ag (CE)	(1×1)	8	42.74	10.73	3.98
Ag (DFT)	(1×1)	8	50.76	14.12	3.59
Ag (CE)	(1×1)	5000	40.30	7.26	5.55
Au (CE)	(1×2)MR	5000	14.43	5.92	2.48

1 M. Bernasconi and E. Tosatti, Surf. Sci. Rep. **17**, 363 (1993).
2 W. A. Harrison, Surf. Sci. **55**, 1 (1976).
3 D. M. Kolb and J. Schneider, Electrochim. Acta **31**, 929 (1986).
4 S. Kitamura, T. Sato, and M. Iwatsuki, Nature **351**, 215 (1991).
5 P. Bak, Solid State Commun. **32**, 581 (1979).
6 J. C. Campuzano, M. S. Foster, G. Jennings, R. F. Willis, and W. Unertl, Phys. Rev. Lett. **54**, 2684 (1985).
7 A. Nduwimana, X. G. Gong, and X. Q. Wang, Appl. Surf. Sci. **219**, 129 (2003).
8 K. M. Ho and K. P. Bohnen, Phys. Rev. Lett. **59**, 1833 (1987).
9 C. H. Lanier, A. van de Walle, N. Erdman, E. Landree, O. Warschkow, A. Kazimirov, K. R. Poeppelmeier, J. Zegenhagen, M. Asta, and L. D. Marks, Phys. Rev. B **76**, 045421 (2007).
10 R. Drautz, H. Reichert, M. Fahnle, H. Dosch, and J. M. Sanchez, Phys. Rev. Lett. **8723**, 236102 (2001).
11 B. C. Han, A. Van der Ven, G. Ceder, and B. J. Hwang, Phys. Rev. B **72**, 205409 (2005).
12 C. Lazo and F. J. Keil, Phys. Rev. B **79** (2009).
13 D. Lerch, O. Wieckhorst, L. Hammer, K. Heinz, and S. Muller, Phys. Rev. B **78**, 121405 (2008).
14 S. Muller, J Phys-Condens Mat **15**, R1429 (2003).
15 J. M. Sanchez, F. Ducastelle, and D. Gratias, Physica A **128**, 334 (1984).
16 A. van de Walle and G. Ceder, J. Phase Equilib. **23**, 348 (2002).
17 J. P. Perdew and Y. Wang, Phys. Rev. B **45**, 13244 (1992).
18 G. L. Kellogg, Phys. Rev. Lett. **55**, 2168 (1985).
19 C. L. Fu and K. M. Ho, Phys. Rev. Lett. **63**, 1617 (1989).
20 K. P. Bohnen and K. M. Ho, Electrochim. Acta **40**, 129 (1995).
21 F. Jensen, F. Besenbacher, E. Laesgaard, and I. Stensgaard, Phys. Rev. B **41**, 10233 (1990).
22 M. Sturmat, R. Koch, and K. H. Rieder, Phys. Rev. Lett. **77**, 5071 (1996).
23 Q. Gao and T. T. Tsong, Phys. Rev. Lett. **57**, 452 (1986).
24 I. K. Robinson, E. Vlieg, and K. Kern, Phys. Rev. Lett. **63**, 2578 (1989).
25 B. P. Burton, A. van de Walle, and U. Kattner, J. Appl. Phys. **100** (2006).
26 A. Van de Walle, Z. Moser, and W. Gasior, Arch. Metall. Mater. **49**, 535 (2004).
27 M. S. Daw and S. M. Foiles, Phys. Rev. Lett. **59**, 2756 (1987).
28 C. Wolverton and V. Ozolins, Phys. Rev. Lett. **86**, 5518 (2001).
29 V. Ozolins, C. Wolverton, and A. Zunger, Phys. Rev. B **58**, R5897 (1998).
30 A. van de Walle and G. Ceder, Rev. Mod. Phys **74**, 11 (2002).
31 S. Wei and M. Y. Chou, Phys. Rev. Lett. **69**, 2799 (1992).
32 C. Wolverton, V. Ozolins, and M. Asta, Phys. Rev. B **69** (2004).
33 K. Morgenstern, E. Laegsgaard, I. Stensgaard, and F. Besenbacher, Phys. Rev. Lett. **83**, 1613 (1999).
34 F. Montalenti and R. Ferrando, Phys. Rev. Lett. **82**, 1498 (1999).